Ordering Lamellar-Forming Copolymer Thin Films in 3D Bicontinuous Morphologies via Lamellar Patterned Substrate

Erukhimovich, I.; Kriksin, Y.; ten Brinke, G.

Published in:
Macromolecules

DOI:
10.1021/acs.macromol.6b02692

Publication date:
2017

Macromolecules

Article

pubs.acs.org/Macromolecules

Ordering Lamellar-Forming Copolymer Thin Films in 3D Bicontinuous Morphologies via Lamellar Patterned Substrate

I. Erukhimovich,[†] Y. Kriksin,[*,‡] and G. ten Brinke[§]

[†]Nesmeyanov Institute of Organoelement Compounds, Russian Academy of Sciences, Moscow 119991, Russia

[‡]Keldysh Institute of Applied Mathematics, Russian Academy of Sciences, Moscow 125047, Russia

[§]Department of Polymer Chemistry and Zernike Institute for Advanced Materials, University of Groningen, Nijenborgh 4, 9747 AG Groningen, The Netherlands

ABSTRACT: The formation of ordered morphologies in thin films of symmetric diblock copolymer melts is considered theoretically. Somewhat surprisingly, under proper boundary conditions the presence of a lamellar chemical pattern on the substrate, being sufficiently pronounced and with the right period, is found to induce the formation of diamond-like morphologies. The phase diagram of the most stable phases on the plane (the substrate period L_x—the film width H) is built within the self-consistent field theory numerical procedure. We also discuss the behavior of the order parameter Fourier spectrum at the transitions between the various morphologies.

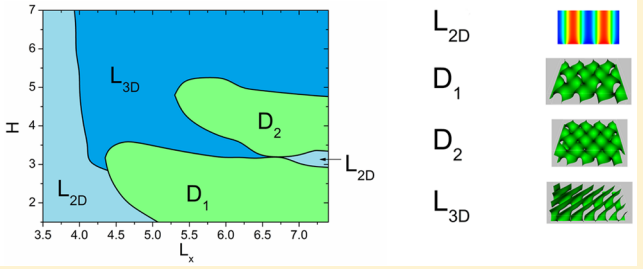

1. INTRODUCTION

Self-assembling of solutions and melts of copolymers into morphologies possessing the symmetry of a crystal lattice,[1−8] which is also called order−disorder transition (ODT) or microphase separation, is one of the most interesting phenomena in polymer science from both a physical and a technological point of view. In particular, the idea to create isoporous membranes based on self-assembling copolymers is relevant in many areas of technology, such as batteries and fuel cells. Accordingly, forming nanostructures in thin films of self-assembling block copolymers[9−16] provides a promising route to produce isoporous membranes.

The conventional ordered morphologies in thin films are the one-dimensional lamellar and two-dimensional hexagonal ones which are characterized by clearly pronounced anisotropic properties. If they are oriented parallel to the film boundaries, which is favored by boundary selectivity, the membrane transport capacity significantly deteriorates as compared to the perpendicular morphologies favored by an increase of the incommensurability between the lamellar period L_b in the bulk and the film width H. A variety of phase diagrams were calculated both on the basis of semi-phenomenological models and theoretical considerations, such as the weak segregation theory (WST) and self-consistent field theory (SCFT).[19−27] Unfortunately, the option to form a mixed morphology comprising both a commensurable parallel and perpendicular lamellar layers within the same film[19] makes the strongly anisotropic thin film morphologies not too stable with respect to keeping good transport properties across the film.[28]

As we suggested recently,[28] a natural route to avoid such a parasitic blocking of the transport in thin films is to make use of nonconventional quasi-isotropic morphologies with e.g. the cubic symmetry rather than the conventional strongly anisotropic 1D and 2D ones. This route is based on the experience gained in the field of morphologies formed in ternary ABC and ABC-like linear block copolymer melts.[29−33] In the bulk the most stable morphologies for symmetric linear block copolymers $A_nB_mC_n$ with a middle block B that is nonselective with respect to the end blocks A and C is depending on the composition $f_B = m/(m + 2n)$, not only the lamellar phase (as in molten diblock copolymers) but also some cubic phases like those possessing the diamond (D) symmetry $fd\bar{3}m$ (space group no. 227), the single (alternating) gyroid (AG) $I4_132$ (space group no. 214), or the simple cubic (SC) $Pn\bar{3}m$ (space group no. 224) one. In some papers[28,32,33] and in what follows the morphologies D, AG, and SC are alternatively designated as D^A, G^A, and S^A, respectively. Remarkably, all of these nonconventional morphologies (especially D and AG) are characterized by the presence of a more or less pronounced bicontinuous cluster of A and C channels,[33] which fits the idea of quasi-isotropic isoporous membranes. Under confinement in a film, the AG morphology is suppressed due to its incompatibility with the reflecting boundary conditions typical in this case,[24,28,33] whereas the D and SC ones become somewhat distorted. Thereby, the most promising (in terms of high permeability) morphologies are the diamond-like ones (DLM); i.e., those possessing the tetragonal and orthorhombic symmetries evolved from the cubic D symmetry as the film confinement effects grow. The reader can find much more detail on the DLM in our recent work.[28] In particular, it was

Received: January 6, 2017
Revised: April 7, 2017
Published: May 10, 2017

DOI: 10.1021/acs.macromol.6b02692
Macromolecules 2017, 50, 3922−3932

shown[28] that the lamellar chemical pattern on a substrate of a proper period can be used to extra stabilize the DLM.

The purpose of the present paper is to demonstrate that the idea to use proper lamellar pattern on a substrate to induce the DLM formation is much more powerful than we supposed at the beginning of our research. In fact, such a pattern can be used to stabilize the DLM in films even for symmetric diblock copolymers, for which the stable phase in the bulk is the lamellar one.

Before validating and demonstrating this idea, it is worth to make two remarks on its advantages. First, if we look at the practical side of membrane production, the simplicity of the technology plays a major role. So, from the viewpoint of ease of processing, it is obviously much simpler to use diblock rather than triblock copolymers. Second, the self-assembly of diblock copolymers on a patterned substrate has been, of course, studied previously (see, e.g., refs 34−38 and references therein). As a rule, in the cases studied until now the stabilized morphology matches the pattern; i.e., a lamellar morphology corresponded to a lamellar pattern, and a hexagonal morphology was stabilized by a hexagonal pattern. One exception is the observation of a kind of bicontinuous morphology (not too well-defined, though) in lamellar-forming diblock copolymers that self-assemble on a 2D patterned substrate.[34] Our study goes further: we show that a proper 1D lamellar-like pattern will induce in symmetric (i.e., lamellar-forming) diblock copolymer films the well-ordered 3D bicontinuous diamond-like morphology (DLM).

The further presentation is organized as follows. In section 2 we remind the reader the basics of the SCFT description of block copolymers in thin films. The results and possible applications are discussed in section 3. The final conclusion is given in section 4.

2. SCFT MODEL AND THE ORDER PARAMETER

Model. Let a diblock copolymer melt fills a film (a slit with parallel plane boundaries $z = 0$ and $z = H$). The melt contains n identical A_kB_l diblock chains with the total degree of polymerization $N = k + l$ and the composition $f = k/N$. The chains are symmetric (both the volume fractions and statistical segments of the A and B blocks are the same and $f = 1/2$). All lengths are measured in the units of the diblock gyration radius R_g. The Flory−Huggins parameter χ describes the incompatibility of the A and B components.

The free energy of the system under consideration reads[7]

$$F/nk_BT = V^{-1}\int d^3\mathbf{r}[\chi N\varphi_A(\mathbf{r})\varphi_B(\mathbf{r}) - w_A(\mathbf{r})\varphi_A(\mathbf{r}) - w_B(\mathbf{r})\varphi_B(\mathbf{r}) + \xi(\mathbf{r})(\varphi_A(\mathbf{r}) + \varphi_B(\mathbf{r}) - 1)] - \ln Q[\{w_A(\mathbf{r}), w_B(\mathbf{r})\}] \quad (1)$$

where V is the volume of the system, k_B is the Boltzmann constant, T is the absolute temperature, $\varphi_\alpha(\mathbf{r})$ is the local volume fraction of the component α, $w_\alpha(\mathbf{r})$ is the field acting on the component α, and $\xi(\mathbf{r})$ is the Lagrange multiplier providing that the incompressibility condition holds.

The quantity $\ln Q[\{w_A(\mathbf{r}),w_B(\mathbf{r})\}]$ appearing in eq 1 is the partition function of a single chain subjected to the fields $\{w_\alpha(\mathbf{r})\}$:

$$Q[\{w_A(\mathbf{r}), w_B(\mathbf{r})\}] = V^{-1}\int d^3\mathbf{r}q(\mathbf{r}, 1) \quad (2)$$

where the integrand $q(\mathbf{r},s)$ satisfies the modified diffusion equation (MDE)

$$\partial q(\mathbf{r}, s)/\partial s = \nabla^2 q(\mathbf{r}, s) - \omega(\mathbf{r}, s)q(\mathbf{r}, s), \quad q(\mathbf{r}, 0) = 1 \quad (3)$$

and the contour variable s ($0 \le s \le 1$) points the position of a monomer unit along the chain.

Now, to state the boundary conditions for eq 3, let us define the elementary cell as the rectangular parallelepiped of dimensions L_x, L_y, and H. The planes $z = 0$ and $z = H$ are respectively the patterned surface (substrate) and the neutral (nonselective with respect to the A and B species) chemically homogeneous one. The periodic boundary conditions with the periods L_x and L_y respectively are imposed on the function $q(\mathbf{r},s)$ in the lateral directions X and Y, and the reflection boundary conditions are applied at both the bottom ($z = 0$) and the top ($z = H$) boundaries.

Surface Field. The function $\omega(\mathbf{r},s)$ in the right-hand side of eq 3 is the sum of the self-consistent $w_\alpha(\mathbf{r})$ and surface $\gamma_\alpha(\mathbf{r})$ fields[28,38,39]

$$\omega(\mathbf{r}, s) = w_{\alpha(s)}(\mathbf{r}) + \gamma_{\alpha(s)}(\mathbf{r}) \quad (4)$$

with $\alpha(s) = A$ if $0 \le s < f$ and $\alpha(s) = B$ if $f \le s < 1$. In general, the surface field $\gamma_\alpha(\mathbf{r})$ describing the effect of a chemical substrate pattern on the diblock copolymer components reads

$$\gamma_\alpha(\mathbf{r}) = \pm 2\varepsilon_{pat}(\mathbf{r}_{pat})\delta(z) \quad (5)$$

where $\mathbf{r}_{pat} = (x, y, 0)$ is the 2D coordinate vector of a point on the substrate S, $\varepsilon_{pat}(\mathbf{r}_{pat})$ is the selectivity profile along the pattern, and the signs "+" and "−" correspond to $\alpha = A$ and $\alpha = B$, respectively. In what follows we assume, for simplicity, that the selectivity profile is a simple harmonic function (for physical meaning of such a profile see ref 28):

$$\gamma_\alpha(\mathbf{r}) = \pm 2\varepsilon \cos(q_p x)\delta(z) \quad (6)$$

where ε is the selectivity amplitude,$q_p = 2\pi/L_p$, and $L_p = L_x$ is the pattern period.

An alternative (but equivalent) way to describe copolymer−substrate coupling is to include into free energy (1) the surface term

$$F_{film} = F + F_S \quad (7)$$

where

$$F_S = -\int d^3\mathbf{r}[\gamma_A(\mathbf{r})\varphi_A(\mathbf{r}) + \gamma_B(\mathbf{r})\varphi_B(\mathbf{r})] = -2\int_S dS\ \varepsilon_{pat}(\mathbf{r}_{pat})\Psi(\mathbf{r}_{pat}) \quad (8)$$

and we introduced the order parameter[28,29]

$$\Psi(\mathbf{r}) = (\varphi_A(\mathbf{r}) - \varphi_B(\mathbf{r}))/2 \quad (9)$$

Thus, the 1D substrate one-harmonic pattern influences only those morphologies, for which the Fourier transform of the order parameter ($\Psi(\mathbf{r})$) cross section by the plane $z = 0$ contains a harmonic (1, 0, 0).

SCFT and Initial Tries. Now we return to the SCFT equations with the incompressibility condition, which read

$$w_A(\mathbf{r}) = \chi N(\varphi_B(\mathbf{r}) - 1 + f) + \xi(\mathbf{r}) \quad (10)$$

$$w_B(\mathbf{r}) = \chi N(\varphi_A(\mathbf{r}) - f) + \xi(\mathbf{r}) \quad (11)$$

DOI: 10.1021/acs.macromol.6b02692
Macromolecules 2017, 50, 3922−3932

Table 1. Main Harmonics and Phase Shifts of the Initial Tries for the Morphologies Relevant in the Bulk

morphology	harmonics	phase shifts
lamella (L)	$\mathbf{q}_1 = \pm q_*(1, 0, 0)$	$\Omega_1 = 0$
diamond (D^A)	$\mathbf{q}_1 = \pm q_*(1,-1,-1)/\sqrt{3}$, $\mathbf{q}_2 = \pm q_*(-1,1,-1)/\sqrt{3}$	$\Omega_1 = 0$, $\Omega_2 = 0$
	$\mathbf{q}_3 = \pm q_*(-1,-1,1)/\sqrt{3}$, $\mathbf{q}_4 = \pm q_*(1,1,1)/\sqrt{3}$	$\Omega_3 = 0$, $\Omega_4 = 0$
single gyroid (G^A)	$\mathbf{q}_1 = \pm q_*(0,1,-1)/\sqrt{2}$, $\mathbf{q}_2 = \pm q_*(-1,0,1)/\sqrt{2}$	$\Omega_1 = \pm\pi/2$, $\Omega_2 = \pm\pi/2$
	$\mathbf{q}_3 = \pm q_*(1,-1,0)/\sqrt{2}$, $\mathbf{q}_4 = \pm q_*(0,-1,-1)/\sqrt{2}$	$\Omega_3 = \pm\pi/2$, $\Omega_4 = 0$
	$\mathbf{q}_5 = \pm q_*(-1,0,-1)/\sqrt{2}$, $\mathbf{q}_6 = \pm q_*(-1,-1,0)/\sqrt{2}$	$\Omega_5 = 0$, $\Omega_6 = 0$
simple cubic (S^A)	$\mathbf{q}_1 = \pm q_*(1,0,0)$, $\mathbf{q}_2 = \pm q_*(0,1,0)$	$\Omega_1 = 0$, $\Omega_2 = 0$
	$\mathbf{q}_3 = \pm q_*(0,0,1)$	$\Omega_3 = 0$

$$\varphi_A(\mathbf{r}) + \varphi_B(\mathbf{r}) = 1 \tag{12}$$

The local volume fractions $\varphi_A(\mathbf{r})$ and $\varphi_B(\mathbf{r})$ can be expressed via the appropriate MDE solutions

$$\varphi_A(\mathbf{r}) = \frac{1}{Q[w_A, w_B]} \int_0^f ds\, q(\mathbf{r}, s)\tilde{q}(\mathbf{r}, 1-s) \tag{13}$$

$$\varphi_B(\mathbf{r}) = \frac{1}{Q[w_A, w_B]} \int_f^1 ds\, q(\mathbf{r}, s)\tilde{q}(\mathbf{r}, 1-s) \tag{14}$$

where the function $\tilde{q}(\mathbf{r},s)$ satisfies the similar MDE

$$\partial\tilde{q}(\mathbf{r}, s)/\partial s = \nabla^2\tilde{q}(\mathbf{r}, s) - \omega(\mathbf{r}, 1-s)\tilde{q}(\mathbf{r}, s), \quad \tilde{q}(\mathbf{r}, 0) = 1 \tag{15}$$

with the boundary conditions discussed after eq 3.

The simultaneous eqs 2−4 and 10−15 describe the state of the diblock melt in a slit with the patterned substrate. To solve these equations, we use iterative methods that optimize the free energy (1) in the same iterative process with respect to the fields $w_\alpha(\mathbf{r})$ and the lateral period L_y.[40] To start the iterative process, it is necessary to chose an initial iteration. Sometimes one uses a random choice of such an initial iteration. We, instead, are applying for this purpose another procedure, which is based on our experience gained within the WST and predetermines the final morphology. For the bulk morphologies the procedure is as follows.

To begin with within the WST,[29] i.e., near the critical point, in the Fourier expansion of the order parameter (9) the main harmonics only are to be taken into account. In other words, the WST order parameter profile (in the bulk) reads

$$\Psi(\mathbf{r}) = A \sum_{|q_k|=q_*} \exp[i(\mathbf{q}_k\mathbf{r} + \Omega_k)] \tag{16}$$

Here $q_* = 2\pi/L_b$ and L_b are the wavenumber and period of the critical order parameter waves in the bulk and the set of the main harmonics $\mathbf{q}_k$, and their phase shifts Ω_k define the morphology type. The sets $\{\mathbf{q}_k\}$ and $\{\Omega_k\}$ for the morphologies relevant are discussed in ref 29 and presented in Table 1.

So, we define the initial iteration specifying the fields $w_\alpha(\mathbf{r})$ in the form (16) with the corresponding main harmonics taken from the Table 1, the initial period L_y being chosen to be equal or close to its value in the bulk. The iterations are stopped when the residuals in the eqs 10−15 (i.e., the accuracy of the fields and component volume fractions) are less than 10^{-4}. The final iteration is considered as the solution of the system of eqs 2−6 and 10−15. When all the solutions are found, we compare the free energies (1) of all competitors (if they exist as metastable phases in a thin film) in order to reveal the morphology with the lowest free energy value.

Initial Tries for the Patterned Films. For the patterned films the situation with the initial tries becomes somewhat more complicated. In general, we expand the order parameter (15) into the Fourier series

$$\Psi(\mathbf{r}) = \sum_{\mathbf{k}} A_{\mathbf{k}} \exp[i(\mathbf{q}_{\mathbf{k}}\mathbf{r} + \Omega_{\mathbf{k}})] \tag{17}$$

where the vectors $\mathbf{q}_{\mathbf{k}}$ run all the nodes of the reciprocal lattice:

$$\mathbf{k} = l\mathbf{e}_x/L_x + m\mathbf{e}_y/L_y + n\mathbf{e}_z/L_z \tag{18}$$

Here L_x, L_y, and L_z are three independent periods along each of the axes; therewith $L_z = 2H$; $L_x = L_p$, $\{\mathbf{e}_\alpha\}$ ($\alpha = x, y, z$) is the orthonormal basis, and $l, m, n = 0, \pm1, \pm2,\ldots$.

In what follows, the triple (l, m, n) specifies the corresponding wave vector $\mathbf{q}_{\mathbf{k}}$. In the intermediate segregation regime the morphology identification can be performed directly through specification of the main and several higher harmonics[28] (see also below subsection on the spectral analysis).

3. RESULTS AND DISCUSSION

A detailed description of the diamond and diamond-like phases and building the corresponding phase diagrams was given previously both microscopically for ternary symmetric ABC-triblock and similar copolymers[29−33] and phenomenologically.[41] Unlike triblock copolymers,[29−33] for symmetric diblock copolymers ($f = 0.5$) in the bulk the diamond and other 3D morphologies mentioned in Table 1 are always metastable only.[28,42] Indeed, as shown in Figure 1 where the free energies for four candidates (L, G^A, D^A, and S^A) calculated in the bulk are presented as the functions of the reduced chi-parameter $\tilde{\chi} = \chi N$, the following chain of inequalities holds: $F_L < F_{G^A} < F_D < F_{SC}$.

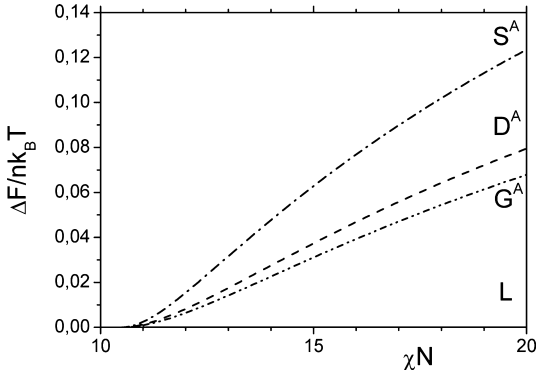

Figure 1. Free energies differences $\Delta F/nk_BT = (F_\alpha - F_L)/nk_BT$ (α = L, G^A, D^A, S^A) as functions of the Flory−Huggins parameter χN: L (solid), G^A (dash-dot-dot) D^A (dash), and S^A (dash-dot) morphologies in the bulk.

DOI: 10.1021/acs.macromol.6b02692
Macromolecules 2017, 50, 3922−3932

But the single (alternating) gyroid morphology G^A cannot be formed under confinement in a film since it does not satisfy geometrical restraints (the G^A phase has no mirror planes and thus cannot be embedded into a slit without considerable distortions[28]). So, in this paper we consider, apart from the conventional lamellar (L), only the remaining diamond (D^A) and simple cubic (S^A) phases found to exist for symmetric ABC copolymers[29−33] (S^A phase exists, of course, for the films with some special dimensions only).

Why Not Just Lamella? The very opportunity that the L phase (more precisely, perpendicular lamella) could become in a film less thermodynamically advantageous than a cubic morphology is unthinkable without introducing an additional (apart from the film itself) constraint, which would increase the L free energy as compared to that of the cubic phase under consideration. It is for this purpose that we introduced the lamellar pattern on the substrate in section 2. Indeed, such a pattern favors the energetic contribution into the perpendicular L but strongly diminishes the entropic one if the pattern period is incommensurable with the natural L period L_b. Taking into account that as we showed earlier[28] the natural period of the diamond morphology along the pattern direction is $\sqrt{3} \approx 1.7$ times higher than L_b (within the weak segregation approximation), we see that such a pattern would distort the D morphology very slightly while the L would be considerably stretched. Therewith, the energetic gains into both D and L morphologies would be the same. Thus, it is the corresponding entropic gain which favors the diamond morphology as compared to the lamellar one. On the other hand, this consideration does not hold for the S^A phase, which exists when the film half-width equals the period L_x, since the characteristic lengths for the S^A and L are about the same (say, $L_{S^A} = 3.69$ and $L_b = 3.63$ at $\tilde{\chi} = 14$ and $\varepsilon = 2$). Summarizing, the actual competition takes place between the lamellar and DLM phases and could be shifted in favor of the DLM via a proper design of the lamellar pattern on the substrate. It is worth to add that adjusting of chain conformations to an external field is a coarse-grain effect, which is therefore determined by the longest waves of the field spectrum. In other words, we expect that it is basically the substrate pattern period rather that other pattern profile details, which influences the relative perpendicular L stability.

Morphologies: Preliminary Overview. Let us first consider the case when the parallel lamellar phase prevails. In the slit with neutral reflecting boundaries, such a phase is dominant only if the slit width is a multiple of the half-period of the lamellar morphology in the bulk. The lamellar pattern on the substrate introduces significant distortions in the parallel lamellar phase. Strictly speaking, this phase becomes a three-dimensional structure due to the fact that the Fourier expansion of the corresponding order parameter includes 3D harmonics belonging to other morphologies. Besides, this phase is only metastable (if it exists) in the range of the film widths used in our calculations.

Now, in the case the period L_x of the lamellar pattern is incommensurable with the period L_b of the lamellar morphology in the bulk, one could think that the inclined lamella with the period equal to L_b wins. But this is not the case since the inclined lamella becomes strongly distorted due to the reflection boundary conditions; the thinner the film is, the more the inclined lamella is distorted (see Figure 2).

As a result, its free energy becomes too high as compared to other competitors. Summarizing, it turns out again that the only

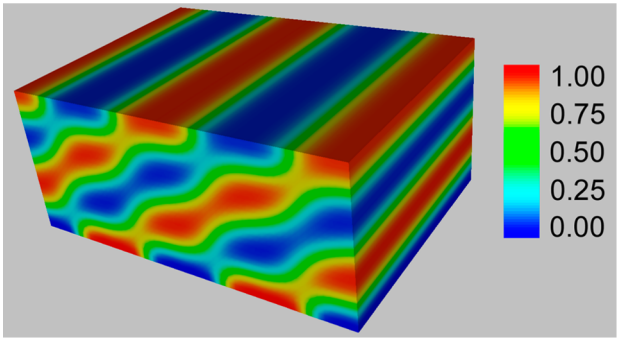

Figure 2. Color visualization of the volume fraction $\varphi_A(\mathbf{r})$ of the metastable inclined lamella at $\tilde{\chi} = 14$, $\varepsilon = 2$, and $H = 6.0$. The top and bottom horizontal planes correspond to the film walls $z = 0$ and $z = H$.

real competitors in thin films are the DLM and the perpendicular lamellar phase. Therewith, the latter is observed in a lamellar patterned film not in a pure form, but rather with an admixture of some extraneous harmonics specific for the DLM. Because of these extra harmonics the perpendicular lamella could look both two-dimensional (2D) and three-dimensional (3D). (A more quantitative definition of these 2D and 3D lamellar-like morphologies (LLM) we designate as L_{2D} and L_{3D}, respectively, will be given below based on the Fourier analysis.)

The characteristic behavior of the free energy as a function of the film width H for the competing LLM (L_{2D} and L_{3D}) and DLM (D_1 and D_2) phases is shown in Figure 3. The index m in the notation D_m indicates the number of DLM half-periods (layers) along the normal to the substrate.[28]

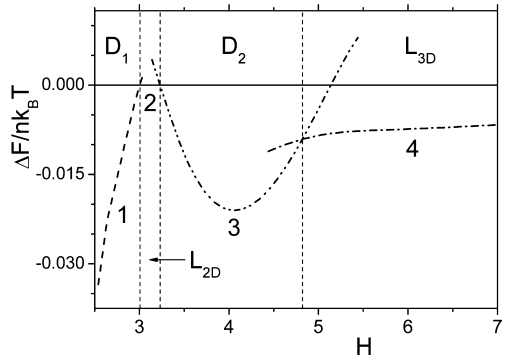

Figure 3. Free energies differences $\Delta F/nk_BT = (F_\alpha - F_{L_{2D}})/nk_BT$ (α = L_{2D}, L_{3D}, D_1, D_2) as functions of the film width H at $L_x = 7.0$. The functions for the D_1, L_{2D}, D_2, and L_{3D} phases are plotted as the dash, solid, dash-dot-dot, and dash-dot curves and labeled by the digits 1, 2, 3, and 4, respectively.

As is seen from Figure 3, the sequence of the stable phases, which replace each other at $L_x = 7.0$ as H increases, is as follows: $D_1 \rightarrow L_{2D} \rightarrow D_2 \rightarrow L_{3D}$. To visualize these morphologies, the corresponding surfaces $\Psi(\mathbf{r}) = 0$ called intermaterial dividing surfaces or IMDS[43] are plotted in Figure 4.

Phase Diagram and Visualization. Calculating the free energy (1) within the SCFT numerical procedure for all competing morphologies L_{2D}, L_{3D}, D_1, and D_2 and comparing their values, we can study how the dominant morphology of the symmetric diblock copolymer thin films is influenced by the selectivity pattern period L_x and film width H (see Figure 5).

DOI: 10.1021/acs.macromol.6b02692
Macromolecules 2017, 50, 3922−3932

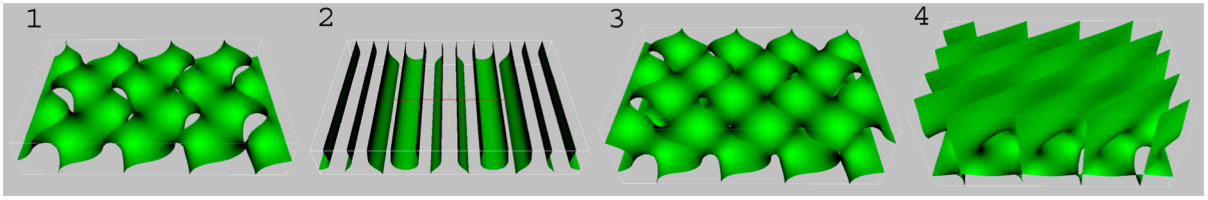

Figure 4. Visualization of various phases at different film width at L_x = 7.0, ε = 2, and $\tilde{\chi}$ = 14. The morphologies D_1 (H = 2.54), L_{2D} (H = 3.14), D_2 (H = 4.54), and L_{3D} (H = 6.04) (labeled by the digits 1, 2, 3 and 4, respectively) are visualized via the intermaterial dividing surfaces ($\varphi_A(\mathbf{r})$ = 0.5). The top and bottom horizontal planes correspond to the film walls z = 0 and z = H.

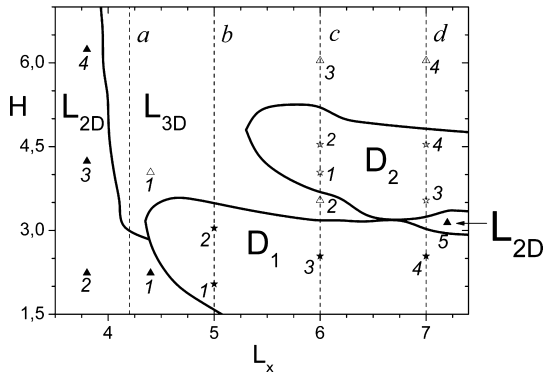

Figure 5. Phase portrait of thin patterned film of the AB diblock copolymers (ε = 2, f = 0.5, $\tilde{\chi}$ = 14). The boundaries between the stability islands of the DLM and L phases are marked by the solid lines. The locations of the numbered solid and open triangles and solid and open stars (the L_{2D}, L_{3D}, D_1, and D_2 phases, respectively) define the L_x and H values for the accordingly numbered morphology images shown in Figures 6–9, respectively. The thin labeled vertical dashed lines correspond to subfigures in Figure 10.

Figures 6–9 give a clear idea of the stable morphologies arising at various periods L_x of the lamellar substrate pattern and film thickness H in the marked points (open and closed triangles and stars in Figure 5). The L_{2D} phase is situated in the left side of the diagram where the pattern period is not much different from the period L_b = 3.63 of the lamellar morphology in the bulk. One more region of the L_{2D} phase is sandwiched between two DLM regions (D_1 and D_2) in the right side of the diagram. We discuss its nature below. The rest of the phase diagram is divided between the DLM and 3D lamellar-like phase L_{3D}. The phase D_1 is located in the lower part of the diagram where the pattern period is incommensurable with the bulk period L_b. So, similar to the situation with the symmetric triblock copolymers,[28] the lamellar phase is suppressed here by the incommensurable lamellar pattern. As the film thickness H increases, the D_1 phase is transformed into the D_2 phase (see the top region of Figure 5). The cause of the D_2 phase formation is that increasing the pattern period makes the geometric dimensions of the elementary cell closer to the size of the diamond elementary cell in the bulk. It could be expected that a further increase in film thickness H would result in the D_3 phase. However, even though the D_3 phase does exist as a metastable solution of the SCFT equations (2)–(6) and (10)–(15) for the values of parameters corresponding to the phase diagram shown in Figure 5, it never becomes dominant here. (One can expect, though, that the number of stable layers will grow as the strength of coupling to the substrate ε increases.) The case is that unlike the symmetric triblock copolymers (of the proper composition), for symmetric diblock copolymers in the bulk the L phase is dominant and the D one is metastable.[42] So, there is a tendency to form the DLM phase near the substrate and the L phase far away from the latter. As a compromise, with increasing film thickness the LLM phase L_{3D} is formed.

Now, there are two ways to visualize the ordered diblock copolymer morphologies. The first one we used already in Figure 4 is to plot the corresponding IMDS, i.e., the surfaces separating the regions with a surplus and shortage of that or another component. The second one we are using now to visualize the typical representatives of the L_{2D} phase in Figure 6

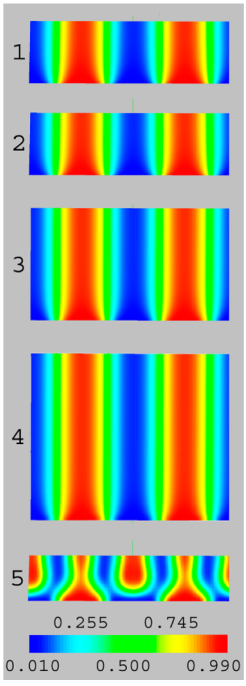

Figure 6. Color visualization of the volume fraction $\varphi_A(\mathbf{r})$ of the stable lamellar-like phase L_{2D}. The pictures are labeled as consistent with the succession of the solid triangles in Figure 5. The top and bottom horizontal lines of color maps correspond to the film walls z = 0 and z = H. To ease the visualization, the corresponding L_{2D} phase period is used as the unit of length in each image 1–5. Accordingly, the actual sizes of the images along both x- and z-axis direction differ from the apparent ones.

is the color visualization, i.e., mapping the spatial distribution of a component volume fraction $\varphi_A(\mathbf{r})$ or the corresponding order parameter, the value of $\varphi_A(\mathbf{r})$ being characterized by a color. As seen from Figure 6, the morphologies for the L_{2D} phases located in the left region of the phase diagram are only little different from the conventional perpendicular lamellar morphology. A slight increase in contrast at the lower part of images 1–4 in Figure 6 corresponding to the closed triangles

DOI: 10.1021/acs.macromol.6b02692
Macromolecules 2017, 50, 3922–3932

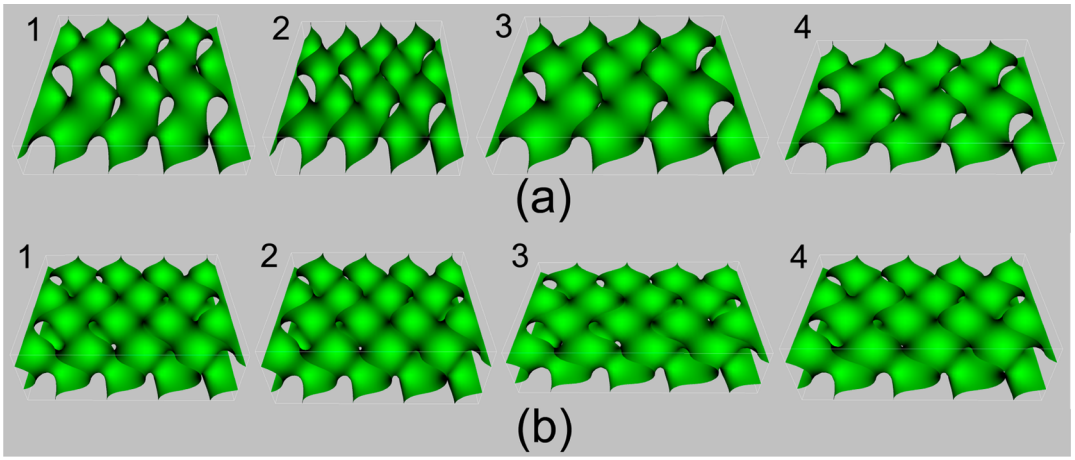

Figure 7. Visualization of the DLM phases via the intermaterial dividing surfaces ($\varphi_A(\mathbf{r}) = 0.5$). The pictures are numbered as consistent with the succession of (a) solid and (b) open stars in Figure 4. The top and bottom horizontal planes correspond to the film walls $z = 0$ and $z = H$.

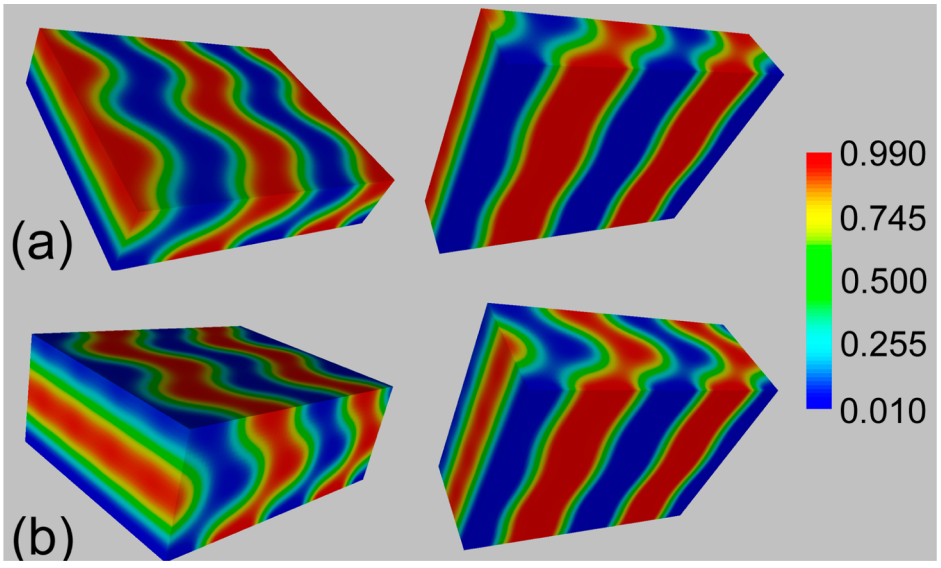

Figure 8. Color visualization of the volume fraction $\varphi_A(\mathbf{r})$ of the stable DLM phases at points marked in Figure 5 by (a) solid star 3 (D_1 phase) and (b) open star 2 (D_2 phase). The top and bottom horizontal planes correspond to the film walls $z = 0$ and $z = H$. On the left and right pictures, the top and bottom sides of the cell are turned toward the viewer, respectively.

1−4 in Figure 5 is obviously due to the patterned substrate influence. A more noticeable distortion of the perpendicular lamellar is observed on the right side of the phase diagram (the solid triangle 5 in Figure 5). As we discuss in more detail in subsection spectral analysis, the peculiarity of this morphology is closely related to the fact that here the pattern period L_x is approximately equal to the doubled period L_b of the lamellar morphology in the bulk. Indeed, this doubling of the pattern period makes a significant disturbance in the distribution of the volume fraction $\varphi_A(\mathbf{r})$ as compared with the first four points (the solid triangles 1−4). However, we still attribute this morphology to the L_{2D} class because, as is seen from Figure 10d, the harmonic (2, 0, 0) corresponding to the lamellar wave with the period close to L_b keeps on to dominate among the other harmonics of the form $(m, 0, n)$.

The most interesting for us are the DLM phases, representatives of which are shown in Figure 7 via the IMDS $\varphi_A(\mathbf{r}) = 0.5$, which reveals the net of intertwined channels characteristic of the DLM.[28,33]

However, the IMDS do not fully characterize the potential permeability of the film. The color map of the volume fraction $\phi_A(\mathbf{r})$ shown in Figure 8 supplements substantially the information provided in Figure 7.

As can be seen from Figure 8, the channel network provides the film permeability in both the longitudinal and transverse directions. What is important, the DLM composed of diblock copolymers are considerably more contrast as compared to symmetric triblocks,[28] in the sense that the span of the volume fraction profile; i.e. the difference between its maximum and minimum is much bigger for diblock copolymers since the value of the volume fraction $\varphi_A(\mathbf{r})$ runs almost the entire allowable range $[0, 1]$. Note also that the domain interfaces are thin enough so that the bulk material (the A and B components) is concentrated directly in the channels. So, etching of one of the film component would provide automatically 50% porosity of the film, the open channels having the quasi-isoporous DLM topology. Comparing the left and right color maps of the volume fraction $\varphi_A(\mathbf{r})$ in Figure 8, one can see a top−bottom asymmetry of the component

DOI: 10.1021/acs.macromol.6b02692
Macromolecules 2017, 50, 3922−3932

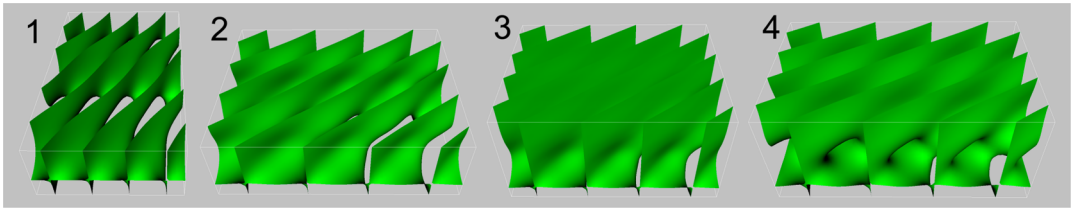

Figure 9. IMDS visualization of the volume fraction $\varphi_A(\mathbf{r})$ of the stable lamellar-like phase L_{3D}. The pictures are labeled as consistent with the succession of the solid triangles in Figure 4. The top and bottom horizontal planes correspond to the film walls $z = 0$ and $z = H$.

Table 2. Key Harmonics Used To Recognize Morphologies

no.	the triple specifying	the morphology relevant		the structure element relevant
1	±(1, 0, 0)	perpendicular L (L_{2D}) phase		the periodic array of layers normal to the x-axis with period L_x
2	±(2, 0, 0)			the periodic array of layers normal to the x-axis with period equal to one-half of L_x
3	±(1, 1, 0)	DLM if the amplitudes of waves 2 and 2′ are the same or hybrid L_{3D} otherwise		periodic tetragonal array of cylinders aligned along the z-axes (perpendicular cylinders)
3′	±(1, −1, 0)			
4	±(1, 0, 1) ±(1, 0, −1)	DLM phases	D_1	a string aligned along the x-axes (one layer) of parallel cylinders, i.e., those directed along the y-axes
5	±(1, 0, 2) ±(1, 0, −2)		D_2	two layers (counted along the z-axes) of parallel cylinders directed along the y-axes
6	±(1, 0, 3) ±(1 ,0, −3)		D_3	three layers (counted along the z-axes) of cylinders directed along the y-axes
7	±(2, 0, 1) ±(2, 0, −1)	perpendicular L_{2D} phase		specific harmonics observable only if $L_x \approx 2L_b$, in which case they are equivalent to harmonics 4
8	±(−1, 1, 1) ±(1, −1, 1)	L_{3D} phase		specific harmonics generated by three-wave coupling of harmonics 1, 2, and 3

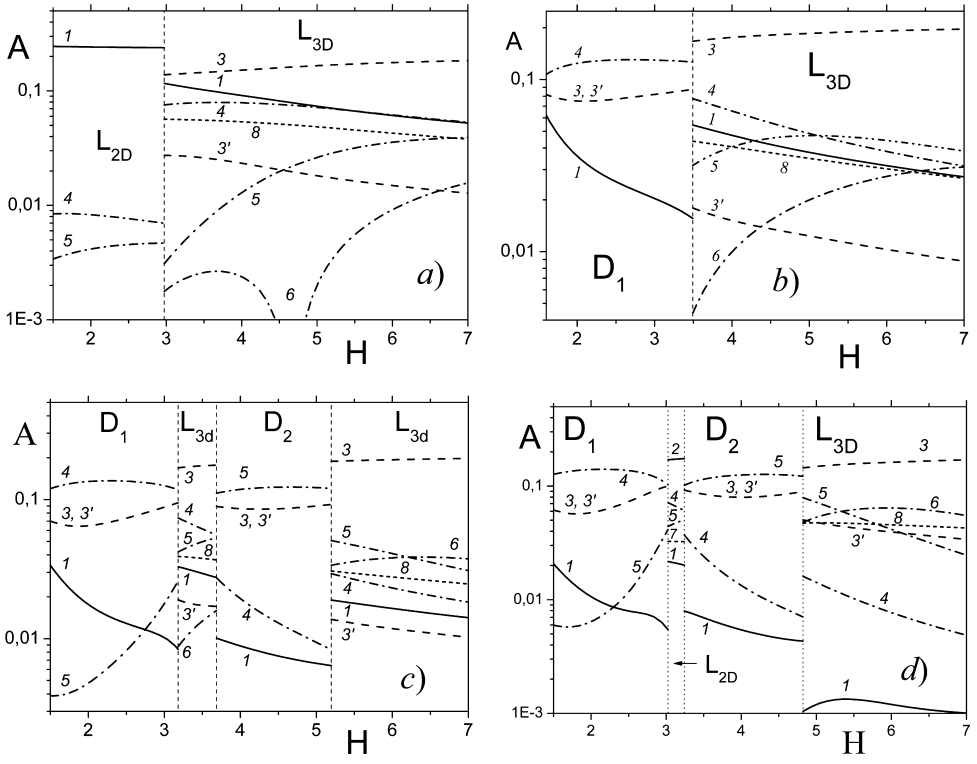

Figure 10. Amplitudes of the most noticeable harmonics of the order parameter (14) as functions of the film width H at $\varepsilon = 2$, $\tilde{\chi} = 14$, and various pattern periods L_x indicated in subfigures, which correspond (in the ascending order) to the vertical lines *a*), *b*), *c*), and *d*) in Figure 6. The harmonics listed in Table 2 that are related to morphologies L_{2D} (1, 2, and 7), D (4, 5, and 6) and L_{3D} (8) are plotted as bold solid, dash-dot, and thin solid lines, respectively. The harmonics 3 and 3′ are plotted by dashed lines. Vertical dotted lines demarcate the phase transition lines.

DOI: 10.1021/acs.macromol.6b02692
Macromolecules 2017, 50, 3922−3932

distribution, which is caused by asymmetry of the patterned substrate and homogeneous film−air surface. The asymmetry is not critical for the film permeability because it does not violate the channel topology.

Now, let us address the last phase L_{3D} shown in the phase diagram (Figure 5). Whereas the solution of the SCFT equations corresponding to the L_{2D} phase has been calculated using the initial iteration for the lamellar harmonics (row 1 of Table 1), that for the L_{3D} phase was found using the initial iteration with the DLM harmonics (row 2 of Table 1). Remarkably, a symmetry breaking occurred in the course of iterations and one of the lateral DLM harmonics is reduced strongly whereas the second one grows stronger than both normal harmonics (we discuss this issue in more detail below when presenting the spectral analysis results). So, the morphology looked as a perpendicular lamella inclined at an angle to the pattern direction, which is in common with a noticeable presence of the main DLM harmonics we see below, a reason to name it the "underdeveloped DLM". Indeed, the IMDS presented in Figure 9 show that near the substrate pattern the L_{3D} resembles the DLM whereas at the top part of the film they are consistent with the idea of the perpendicular lamellar phase. The thicker the film is, the more similar the top part is to the conventional lamellar phase. One more interesting feature of the L_{3D} phase is that optimization of the free energy (1) with respect to the value of the transversal period L_y leads to the L_{3D} period coinciding with the lamellar period L_b with a very good accuracy (less than 1%). Summarizing, the "underdeveloped DLM" phase L_{3D} belongs to a pronounced hybrid type that combines the properties of the DLM and lamella like a centaur or chimera.

Phase Diagram and Spectral Analysis. To provide a more quantitative description of the morphologies visualized above, we perform the order parameter Fourier analysis (the spectral analysis), which is one of the most accurate methods to identify structures. For this purpose we expand the order parameter (9) into the Fourier series (17) where the vectors $\mathbf{q}_k$ run all the nodes of the reciprocal lattice (18).

In what follows, the triple (l, m, n) specifies the corresponding wave vector $\mathbf{q}_k$. In the intermediate segregation regime the morphology identification can be performed directly through specification of the main and several higher harmonics as it was implemented under analyzing structures in films of symmetric triblock copolymers.[28]

To start, we list the most noticeable harmonics to be taken into account for a more accurate recognition of the stable morphologies in the phase diagram shown in Figure 5 (see also ref 26):

Monitoring how are the amplitudes A_q of the harmonics listed in Table 2 changing with increasing the film width H (see Figure 10) provides valuable information on the morphologies. To demonstrate it, let us follow the procedure presented previously[28] and plot A_q of the noticeable harmonics as functions of the film width H at various values of the pattern period L_x. The plots are to be compared with the phase portrait shown in Figure 5.

A general feature of all subfigures in Figure 10 is the presence of jump-like changes of the calculated spectra at certain threshold values of the film thickness H. These changes are determined by the spatial component density rearrangements under order−order transitions between the competing morphologies and, accordingly, the threshold values correspond to equality of the free energies (1) calculated for the competing morphologies. One can see from Figure 10 that the L_{2D} morphology is, indeed, characterized by the dominant lamellar harmonic of the period $L_x \sim L_b$ (harmonics 1 and 2 in Figures 10a and 9d, respectively), with the wave vector aligned along the normal to the pattern layers. On the contrary, the L_{3D} morphology is basically determined by the dominant lamellar harmonic 3, which is the only lateral diamond-like harmonic that survived safely the symmetry breaking (the amplitude of the conjugated harmonic 3′ is much less). It is seen from Figures 10a and 10b also that the relative (with respect to all other harmonics) amplitude of the inclined (with respect to the lamellar pattern direction) harmonic 3 is noticeably less than that of the conventional perpendicular harmonic 1. However, the relative amplitude of harmonic 3 is certainly greater than those of all other harmonics, and it increases with increase of the film thickness H. One should notice also that the number of other (nondominant) harmonics observable for L_{3D} is greater than that for L_{2D}. Thus, the spectral data strongly support the idea that the L_{3D} morphology is a sort of a special hybrid morphology that is to be differentiated from both the DLM and conventional perpendicular lamella L_{2D}.

As the pattern period L_x increases, the DLM morphologies become more common. Say, for L_x = 5.0 (see Figure 10b) we see a region of the one-layer DLM phase D_1, which is characterized by the presence of both lateral (3) and normal (4) diamond-like harmonics, whose intensity is superior with respect to lamellar harmonic (1). The inequality of the amplitudes of the harmonics 3 and 4, which is clearly seen in Figure 10b−d, implies that the actual symmetry of the corresponding DLM is orthorhombic.[28] The further increase of L_x and H results in replacement of the D_1 morphology by D_2, which is manifested by the corresponding replacement of the harmonic 4 by that 5.

Some peculiarities of the L−D competition are revealed by the spectral data shown in Figure 10d where a sort of resonance $L_x \approx 2L_b$ (between the natural L period L_b and the pattern period L_x) occurs, which is expected to favor the L phase. Nevertheless, the L exists in a narrow interval of the film widths only where the harmonic 2 dominates, while the DLM and L_{3D} phases win out of this interval. The case is that there is still a noticeable distortion of the L phase due to necessity to reorganize lamella from the doubled period L_x on the substrate to the ordinary one L_b on the free film surface. A similar reorganization (a weaker one, though) occurs for the DLM either. But what is important, the energetic gain due to coupling between the inhomogeneous spatial distribution of the order parameter and substrate pattern for the L with the doubled period is much less than for that with the ordinary one. Indeed, it follows from eq 8 that the strong harmonic 2 is not coupled to the substrate pattern at all whereas the coupled harmonic 1 is weak. On the contrary, all the DLM harmonics stay energetically coupled to the pattern. Summarizing, a subtle balance between the entropic and energetic gains accompanying the doubling of the L period and the corresponding order parameter reorganization depends heavily from both the film width and pattern period.

Weak vs Strong Segregation and Surface Selectivity vs bulk Incompatibility. Now, before to proceed to Conclusion and summarize our results, it makes sense to address one more important issue, which one of our referees stated as follows: *"the calculations are restricted by a regime of weak enough segregation (χN = 14), which is less interesting for potential applications than the strong segregation regime"*.

DOI: 10.1021/acs.macromol.6b02692
Macromolecules 2017, 50, 3922−3932

To find how much segregated is our diblock copolymer in fact, we present profiles of the volume fraction ϕ_A for the lamellar phase L_{2D} in Figure 11 at various values of the reduced

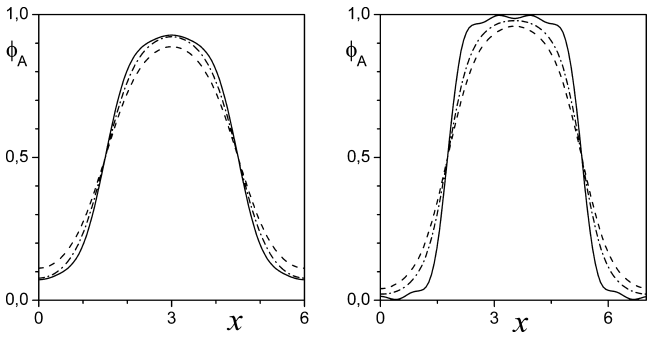

Figure 11. Profiles $\phi_A(x)$ plotted within one period of the lamellar pattern ($0 \le x \le L_x$) for three relative widths $z = 0.1H$ (solid), $z = 0.5H$ (dash), and $z = 0.9H$ (dash-dot) (H is the total film width). Left: $\varepsilon = 2$, $\tilde{\chi} = 14$, $H = 6.04$, $L_x = 6.0$, $y = 2.31$. Right: $\varepsilon = 15$, $\tilde{\chi} = 20$, $H = 2.38$, $L_x = 7.0$, $y = 2.54$.

incompatibility $\tilde{\chi} = \chi N$ and the surface selectivity ε. One can see from Figure 11 that it is not easily to decide whether the system is weakly or strongly segregated at $\tilde{\chi} = 14$ and $\tilde{\chi} = 20$. In both cases the profiles are rather smeared (as expected for weak segregation) whereas the segregation at extrema is almost complete (as expected for strong segregation). The case is that the *naive* idea of strongly segregated block copolymer morphologies with narrow interfaces between domains filled by different repeated units is much less suitable for potential applications than it is commonly believed. Indeed, if we take the relative width of the interface $\delta = D/L$ (where D is the width of the interface and L is the domain size) as a natural measure of the segregation degree ($\delta \sim 1$ and $\delta \to 0$ for weak and strong segregation, respectively), then one can estimate[44] that $\delta \sim \tilde{\chi}^{-2/9}$. In other words, the commonly expected strong segregation with narrow interfaces could be expected only for so low temperatures (high $\tilde{\chi}$) where glassing and slow equilibration would question any reasonable comparison between theory and experiment. Thus, we believe that our SCFT consideration is really rather relevant for potential applications.

Generally, an increase in parameter $\tilde{\chi}$ favors the lamellar phase. However, the presence of a chemical pattern on the substrate fundamentally changes the equilibrium between various morphologies and increase of the selectivity amplitude ε favors the DLM. To compare these competing effects, we also performed the SCFT-based calculation at $\tilde{\chi} = 20$ and different values of ε. The result is represented in Figure 12.

As can be seen from Figure 12a, increasing of the parameter $\tilde{\chi}$ results in a loss of the D_2 phase stability, the D_1 phase being remained stable. As a result, the D_2 phase is replaced by the L_{3D} phase. Figure 10b shows that an increase in the parameter ε leads to a recovery of the D_2 phase stability whereas the D_1 phase stability region broadens somewhat. Thus, the resulting microphase separation is determined not only by the degree of segregation, but rather by the compromise between the incompatibility of different monomers and the strength of interaction of chains with the substrate pattern.

4. CONCLUSION

To summarize, in the present paper we advanced further along the new route toward efficient block copolymer membranes we suggested recently.

1. On the basis of our experience in the field of ternary ABC block copolymers,[29−33] we suggested earlier[28] to use for producing quasi-isoporous membranes the ternary symmetric ABC block copolymers of a special composition with the middle block nonselective with respect to the end blocks because the stable ordered phase in the bulk for such copolymers is known to possess a diamond-like symmetry.
2. In this paper we presented, based on what we call "WST-guided SCFT",[28−31,33] new self-consistent field theory calculations which show that the stable (rather than metastable only) diamond-like morphologies can be formed in symmetric (lamellar-forming) diblock copolymers as well, which makes producing quasi-isoporous membranes much more practicable.
3. The DLM morphologies in thin films, which for lamellar-forming block copolymers in the bulk are usually metastable only, can be stabilized by inducing the germ waves with the proper wavelength via imprinting the lamellar-like pattern on the substrate and subsequent coupling of these germ waves with the virtual parallel cylinder-like structures formed below the ordering spinodal.

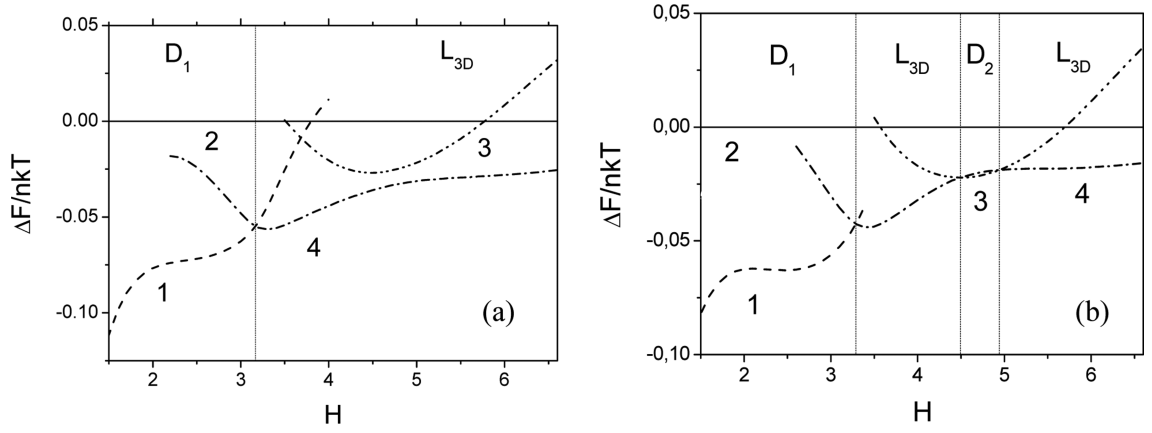

Figure 12. Free energies differences $\Delta F/nk_BT = (F_\alpha - F_{L_{2D}})/nk_BT$ ($\alpha = L_{2D}$, L_{3D}, D_1, D_2) for $\varepsilon = 2$ (a) and $\varepsilon = 15$ (b) as functions of the film width H at $L_x = 7.0$ and $\tilde{\chi} = 20$. The functions for the D_1, L_{2D}, D_2, and L_{3D} phases respectively are singled out as the dash, solid, dash-dot-dot, and dash-dot curves and labeled by the digits 1, 2, 3, and 4.

DOI: 10.1021/acs.macromol.6b02692
Macromolecules 2017, 50, 3922−3932

4. Unlike the DLM in triblock copolymers, those in diblock ones are of a substantially more contrasting structures. Because of the lack of the middle block, the A and B volume fractions can run practically any values between 0 and 1, which will facilitate more easy etching of one of the components to obtain a bicontinuous porous medium.

5. The strength of the coupling between block copolymers and the lamellar pattern on the substrate is very essential. So, one of the issues we suppose to study elsewhere is how much can we control the strength (e.g., via making reversible cross-links between block copolymer and pattern).

AUTHOR INFORMATION

Corresponding Author

*E-mail kriksin@imamod.ru (Y.K.).

ORCID

I. Erukhimovich: 0000-0001-5550-7173

Y. Kriksin: 0000-0002-3840-4874

Notes

The authors declare no competing financial interest.

ACKNOWLEDGMENTS

We thank Profs. P. G. Khalatur and A. N. Semenov for useful discussions and our unknown referees for thoughtful comments. SCFT calculations have been performed under assistance of the Center for Information Technology of the University of Groningen and the Research Computing Center of M.V. Lomonosov Moscow State University. Y.K. is grateful also for financial support from RFBR (Project No. 16-03-00223).

REFERENCES

(1) Bates, F. S.; Fredrickson, G. H. Block Copolymer Thermodynamics: Theory and Experiment. *Annu. Rev. Phys. Chem.* **1990**, *41*, 525−557.

(2) Erukhimovich, I. YA.; Khokhlov, A. R. Microphase Separation in Polymer Systems: New Approaches and Systems. *Polym. Sci., Ser. A* **1993**, *35*, 1522−1531.

(3) Binder, K. Phase transitions in polymer blends and block copolymer melts: Some recent developments. *Adv. Polym. Sci.* **1994**, *112*, 181−299.

(4) Bates, F. S.; Fredrickson, G. H. Block Copolymers—Designer Soft Materials. *Phys. Today* **1999**, *52*, 32−38.

(5) *Supramolecular Polymers*; Ciferri, A., Ed.; Dekker: New York, 2000.

(6) *Block Copolymers in Nanoscience*; Lazzari, M., Liu, G., Lecommandoux, S., Eds.; Wiley-VCH: New York, 2006.

(7) Fredrickson, G. H. *The Equilibrium Theory of Inhomogeneous Polymers*; Oxford University Press: New York, 2006.

(8) Nanostructured Soft Matter: Experiment, Theory, Simulation and Perspectives. In *NanoScience and Technology*; Zvelindovsky, A. V., Ed.; Springer: New York, 2007.

(9) Binder, K. Phase Transitions of Polymer Blends and Block Copolymer Melts in Thin Films. *Adv. Polym. Sci.* **1999**, *138*, 1−89.

(10) Fasolka, M. J.; Mayes, A. M. Block Copolymer Thin Films: Physics and Applications. *Annu. Rev. Mater. Res.* **2001**, *31*, 323−355.

(11) Wang, Q. In *Nanostructured Soft Matter*; Zvelindovsky, A. V., Ed.; Springer: Netherlands, 2007; p 495.

(12) Peinemann, K. V.; Abetz, V.; Simon, P. F. Asymmetric superstructure formed in a block copolymer via phase separation. *Nat. Mater.* **2007**, *6*, 992−996.

(13) Wang, J.-Y.; Chen, W.; Russell, T. P. Patterning with block copolymers. In *Unconventional Nanopatterning Techniques and Applications*; Rogers, J. A., Lee, H. H., Eds.; Wiley: Hoboken, NJ, 2009; pp 233−289.

(14) Phillip, W. A.; O'Neill, B.; Rodwogin, M.; Hillmyer, M. A.; Cussler, E. L. Self-Assembled Block Copolymer Thin Films as Water Filtration Membranes. *ACS Appl. Mater. Interfaces* **2010**, *2*, 847−853.

(15) Jackson, E. A.; Hillmyer, M. A. Nanoporous Membranes Derived from Block Copolymers: From Drug Delivery to Water Filtration. *ACS Nano* **2010**, *4*, 3548−3553.

(16) Rangou, S.; Buhr, K.; Filiz, V.; Clodt, J. I.; Lademann, B.; Hahn, J.; Jung, A.; Abetz, V. Self-organized isoporous membranes with tailored pore sizes. *J. Membr. Sci.* **2014**, *451*, 266−275.

(17) Abetz, V. Isoporous Block Copolymer Membranes. *Macromol. Rapid Commun.* **2015**, *36*, 10−22.

(18) Gunkel, I.; Gu, X.; Sun, Z.; Schaible, E.; Hexemer, A.; Russell, T. P. An In Situ GISAXS Study of Selective Solvent Vapor Annealing in Thin Block Copolymer Films: Symmetry Breaking of In-Plane Sphere Order upon Deswelling. *J. Polym. Sci., Part B: Polym. Phys.* **2016**, *54*, 331−338.

(19) Matsen, M. Thin films of block copolymer. *J. Chem. Phys.* **1997**, *106*, 7781−7791.

(20) Geisinger, T.; Müller, M.; Binder, K. Symmetric diblock copolymers in thin films. I. Phase stability in self-consistent field calculations and Monte Carlo simulations. *J. Chem. Phys.* **1999**, *111*, 5241−5250.

(21) Wang, Q.; Yan, Q. L.; Nealey, P. F.; de Pablo, J. J. Monte Carlo simulations of diblock copolymer thin films confined between two homogeneous surfaces. *J. Chem. Phys.* **2000**, *112*, 450−464.

(22) Huinink, H. P.; Brokken-Zijp, J. C. M.; van Dijk, M. A.; Sevink, G. J. A. Asymmetric block copolymers confined in a thin film. *J. Chem. Phys.* **2000**, *112*, 2452−2462.

(23) Tsori, Y.; Andelman, D. Diblock copolymer thin films: Parallel and perpendicular lamellar phases in the weak segregation limit. *Eur. Phys. J. E: Soft Matter Biol. Phys.* **2001**, *5*, 605−614.

(24) Angerman, H. J.; Johner, A.; Semenov, A. N. Microphase Separation in Thin Block Copolymer Films: A Weak Segregation Mean-Field Approach. *Macromolecules* **2006**, *39*, 6210−6220.

(25) Szamel, G.; Müller, M. Thin films of asymmetric triblock copolymers: A Monte Carlo study. *J. Chem. Phys.* **2003**, *118*, 905−913.

(26) Li, W.; Liu, M.; Qiu, F.; Shi, A.-C. Phase Diagram of Diblock Copolymers Confined in Thin Films. *J. Phys. Chem. B* **2013**, *117*, 5280−5288.

(27) Knoll, A.; Horvat, A.; Lyakhova, K. S.; Krausch, G.; Sevink, G. J. A.; Zvelindovsky, A. V.; Magerle, R. Phase Behavior in Thin Films of Cylinder-Forming Block Copolymers. *Phys. Rev. Lett.* **2002**, *89*, 035501.

(28) Erukhimovich, I. YA.; Kriksin, Yu. A.; ten Brinke, G. Diamond-Forming Block Copolymers and Diamond-like Morphologies: A New Route toward Efficient Block Copolymer Membranes. *Macromolecules* **2015**, *48*, 7909−7922.

(29) Erukhimovich, I. Y. Weak segregation theory and non-conventional morphologies in the ternary ABC triblock copolymers. *Eur. Phys. J. E: Soft Matter Biol. Phys.* **2005**, *18*, 383−406.

(30) Smirnova, Yu. G.; ten Brinke, G.; Erukhimovich, I. YA. Microphase separation in multiblock copolymer melts: Nonconventional morphologies and two-length-scale switching. *J. Chem. Phys.* **2006**, *124*, 054907.

(31) Kriksin, Yu. A.; Erukhimovich, I. YA.; Khalatur, P. G.; Smirnova, Yu. G.; ten Brinke, G. Nonconventional morphologies in two-length scale block copolymer systems beyond the weak segregation theory. *J. Chem. Phys.* **2008**, *128*, 244903.

(32) Qin, J.; Bates, F. S.; Morse, D. C. Phase Behavior of Nonfrustrated ABC Triblock Copolymers: Weak and Intermediate Segregation. *Macromolecules* **2010**, *43*, 5128−5136.

(33) Erukhimovich, I. YA.; Kriksin, Yu. A.; ten Brinke, G. The diamond and other non-conventional morphologies in two-scale multiblock AB copolymers. *Soft Matter* **2012**, *8*, 2159−2169.

(34) Daoulas, K. C.; Mueller, M.; Stoykovich, M. P.; Park, S.-M.; Papakonstantopoulos, Y. J.; de Pablo, J. J.; Nealey, P. F.; Solak, H. H. Fabrication of Complex Three-Dimensional Nanostructures from Self-Assembling Block Copolymer Materials on Two-Dimensional Chemi-

DOI: 10.1021/acs.macromol.6b02692
Macromolecules 2017, 50, 3922−3932

cally Patterned Templates with Mismatched Symmetry. *Phys. Rev. Lett.* **2006**, *96*, 036104.
(35) Detcheverry, F. A.; Nealey, P. F.; de Pablo, J. J. Directed Assembly of a Cylinder-Forming Diblock Copolymer: Topographic and Chemical Patterns. *Macromolecules* **2010**, *43*, 6495−6504.
(36) Detcheverry, F. A.; Pike, D. Q.; Nealey, P. F.; Mueller, M.; de Pablo, J. J. Simulations of theoretically informed coarse grain models of polymeric systems. *Faraday Discuss.* **2010**, *144*, 111−125.
(37) Nagpal, U.; Kang, H.; Craig, G. S. W.; Nealey, P. F.; de Pablo, J. J. Pattern Dimensions and Feature Shapes of Ternary Blends of Block Copolymer and Low Molecular Weight Homopolymers Directed To Assemble on Chemically Nanopatterned Surfaces. *ACS Nano* **2011**, *5*, 5673−5682.
(38) Kriksin, Yu. A.; Khalatur, P. G.; Neratova, I. V.; Khokhlov, A. R.; Tsarkova, L. A. Directed Assembly of Block Copolymers by Sparsely Patterned Substrates. *J. Phys. Chem. C* **2011**, *115*, 25185−25200.
(39) Petera, D.; Muthukumar, M. Self-consistent field theory of diblock copolymer melts at patterned surfaces. *J. Chem. Phys.* **1998**, *109*, 5101−5107.
(40) Kriksin, Y. A.; Khalatur, P. G. Parallel Algorithm for 3D SCF Simulation of Copolymers With Flexible and Rigid Blocks. *Macromol. Theory Simul.* **2012**, *21*, 382−399.
(41) Erukhimovich, I.YA. Symmetry of Gyroid and Weak Crystallization Phase Diagram. *JETP Lett.* **1996**, *63*, 459−463.
(42) Leibler, L. Theory of Microphase Separation in Block Copolymers. *Macromolecules* **1980**, *13*, 1602−1617.
(43) Wohlgemuth, M.; Yufa, N.; Hoffman, J.; Thomas, E. I. Triply Periodic Bicontinuous Cubic Microdomain Morphologies by Symmetries. *Macromolecules* **2001**, *34*, 6083−6089.
(44) Likhtman, A. E.; Semenov, A. N. An Advance in the Theory of Strongly Segregated Polymers. *Europhys. Lett.* **2000**, *51*, 307−313.

DOI: 10.1021/acs.macromol.6b02692
Macromolecules 2017, 50, 3922−3932